11 Molecular Dynamics Simulation of Surfactant Monolayers

Bin Liu, Jirasak Wong-Ekkabut, and Mikko Karttunen

CONTENTS

11.1 INTRODUCTION

In this chapter, we provide a brief introduction to molecular simulations of lipid/surfactant monolayers. We do not aim to provide a comprehensive review. Instead, we first discuss the very timely problem of nanoparticle interactions with the lung surfactant and how that can be studied by simulations. After that, we provide a detailed introduction on the various aspects of building a monolayer simulation and show a case study using simulations of cationic surfactants and zwitterionic lipids. The aim is to provide the reader with a detailed view of how to build simulations, what aspects are important, and what kind of properties can be analyzed. In our other contributions of this volume, we discuss electrostatic interactions in detail (see Chapter 6). That discussion is also valid here and we refer the reader to Chapter 6 regarding the details of how the important electrostatic interactions must be accounted for in interfacial systems.

11.2 EFFECT OF CARBON NANOPARTICLES ON LUNG SURFACTANT

Continuous combustion of fossil fuel produces airborne pollutants into the atmosphere. To a large degree, pollutants consist of carbonaceous particles with a broad size distribution [1–4]. Usually, larger particles can be trapped and removed from the respiratory system, while the smaller ones, especially those in the nanometer range, can reach the alveoli and get transferred into the blood circulatory system [5–7]. Therefore, these combustion-generated particles are responsible for various respiratory and cardiovascular diseases [5,8,9]. There have been growing public health concerns regarding nanomaterials, and the potential risk issues associated with carbon nanoparticles (CNPs) have been intensely studied. It has been known for some time that CNPs deposit in the lung and can induce pneumoconiosis [10–15].

Computer simulations provide an approach to investigate the molecular-level interactions of nanoparticles with the lung surfactant. Importantly, simulations results can predict how nanoparticles influence hydrogen bonding, hydrophobic interactions, and ordering of the lung surfactant.

This allows for detailed analysis of the structural and dynamic properties of lung surfactant in the presence of varying concentrations of CNPs. In reality, the lung surfactant consists of various biological molecules, for example, phospholipids, cholesterol, and surfactant protein [16]. The inclusion of all of the components is impossible, since simulations are limited by the number of molecules they can handle as well as accessible time scales. To reduce the complexity of the system, pure lipid monolayer of dipalmitoylphosphatidylcholine (DPPC) and fullerene C60 have been used in a number of studies as a simple model of lung surfactant and CNPs, respectively. In our own study using such a system, coarse-grained molecular dynamics (CGMD) simulations with the Martini force field [17] were performed with a series of constant particle number, volume and temperature (NVT) simulations with various box sizes at C60:DPPC ratios up to 0.3 [18]. CGMD allow us to reach a reasonably large length and long time scales (the systems consisted of 1600 molecules per monolayer and run for 5–10 μs) so that monolayer collapse and pore formation could be observed [19,18]. In the presence of fullerenes, the surface tensions of monolayers significantly decreased at high compression (at small area per molecule), resulting in collapse of the monolayer, as shown in Figure 11.1. This is in agreement with the results from simulations of ternary lipid mixture monolayers [20]. On the other hand, at low compression (at a large area per molecule), fullerenes increase the surface tension of a monolayer, leading to pore formation, as shown in Figure 11.2. Interestingly, the monomeric fullerene had been suggested to be a stable form in both lipid monolayer and bilayer [14,21]. This result is, however, reliable only at low compression. Study of aggregation of fullerenes in monolayer showed that monomeric fullerene becomes significantly less especially at high compression and high concentration of fullerenes, Figure 11.3; see Ref. [18]. Aggregation of fullerenes causes a decrease of the effective area per molecule and lower surface tension. When fullerene clusters become larger in size than the monolayer thickness; the monolayer bends and folds into a bilayer/a hemispherical budding structure to prevent exposure to the vapor and water phase as shown in Figure 11.1. The free energy calculations [18] of a single fullerene transferring across the monolayer suggest that fullerene can easily penetrate into lipid monolayers and spontaneous translocation of fullerene out of the monolayer is rather difficult.

In conclusion, the simulations were able to suggest that the potentially harmful effects of the deposited CNPs on the respiratory system might be related to the difficulty of CNP clearance from lung surfactant. In addition, simulations suggest that CNPs may alter the physical and mechanical properties of lung surfactant [20,18], which are responsible for respiratory distress syndrome [20,22–25].

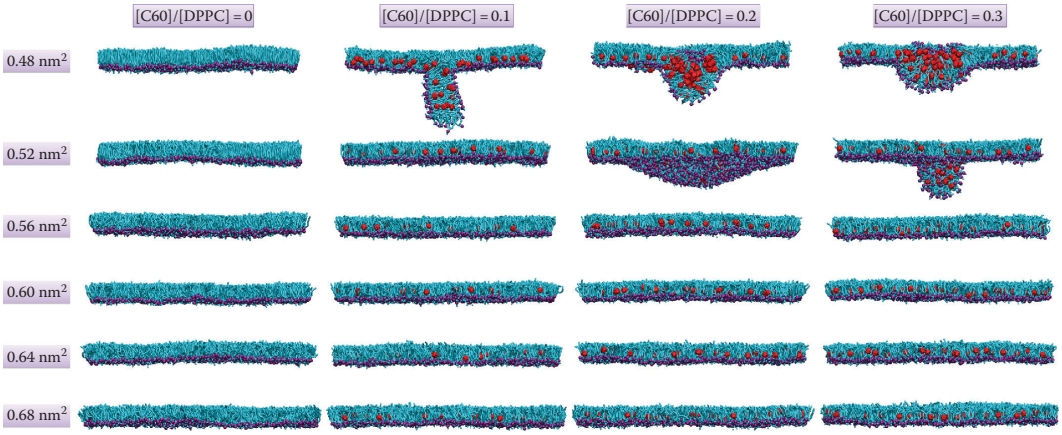

FIGURE 11.1 Snapshots illustrating the equilibrium systems of 1600 molecules/monolayer in the *xz*-plane. Cyan: lipid tails, purple: phosphate group in lipid heads, and red: fullerene. Water was omitted for clarity.

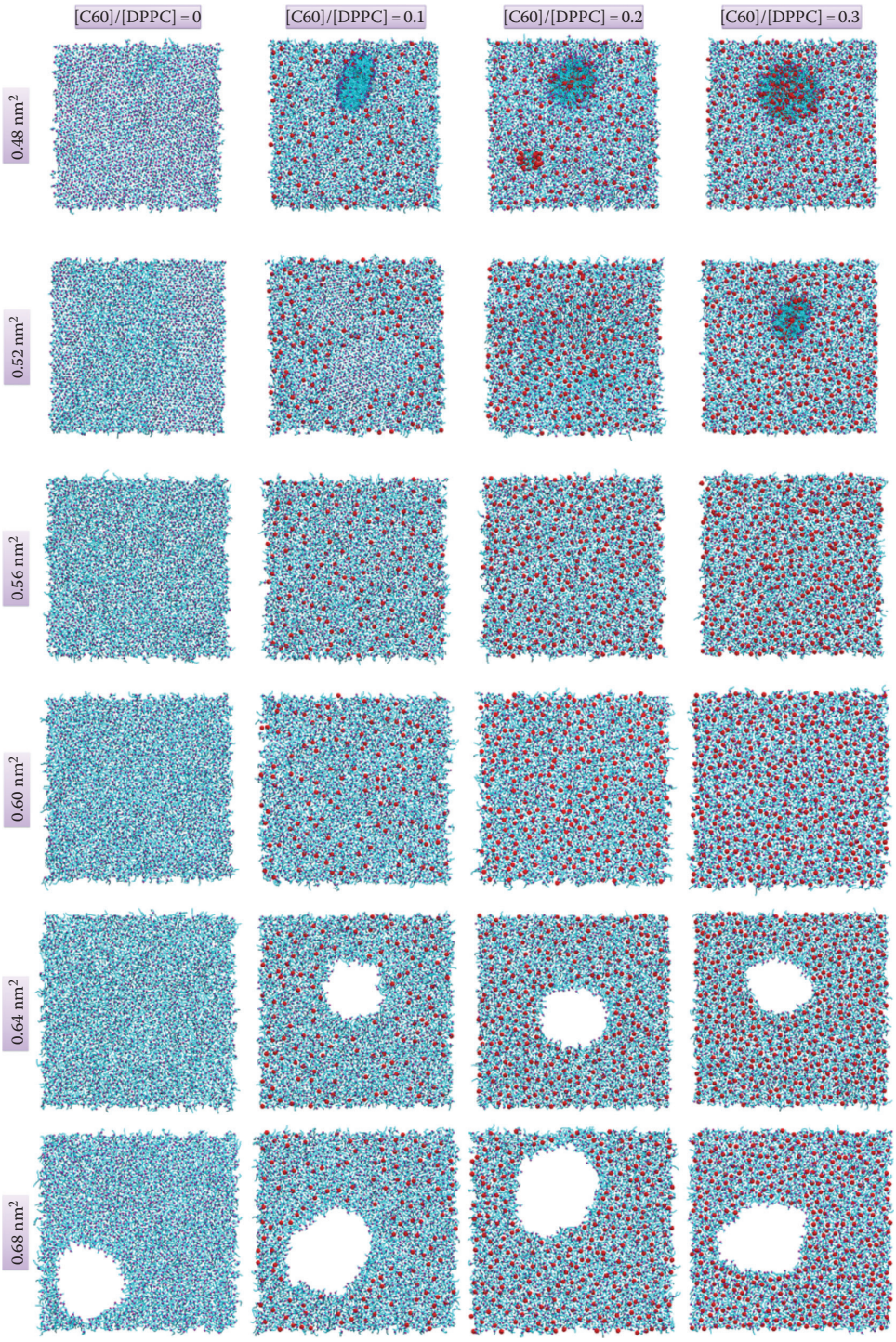

FIGURE 11.2 Snapshots illustrating the equilibrium systems of 1600 molecules/monolayer in the *xy*-plane. Colors and simulation time are the same as in Figure 11.1.

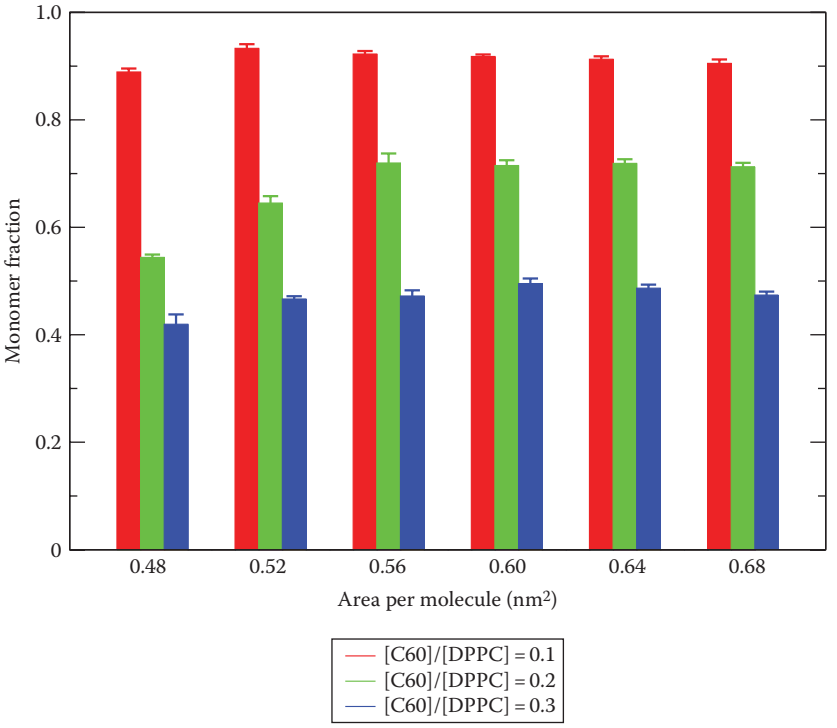

FIGURE 11.3 The monomer fraction of fullerenes as a function of the area per molecule at [C60]/[DPPC] ratios of 0.1 (red), 0.2 (green), and 0.3 (blue).

11.3 PARAMETRIZING LIPID MOLECULES

Section 11.2 demonstrated the utility of molecular simulations. In this section, we discuss the details of how to obtain parameters for lipid or surfactant molecules when they are not readily available from prior research.

Before being able to perform any MD simulations, one must obtain force fi eld parameters, or in case they do not exist, parametrize the molecules of interest so that the MD program can understand their compositions, structures, and interactions with each other and other components in simulation. This is an essential step as it determines the simulation's correctness, quality, and value. Although lots of lipid and surfactant molecules have been parameterized, for many lipid molecules, signi - cant manual work, including *ab initio* calculations for partial charges and constructing topology fi les which describe the modeling or parametrization understandable to a MD program, is still mandatory to obtain a quality parametrization for lipid molecules. Tools for generating topology fi les automatically from a structure fi le such as a PDB fi le exist [26]. But the quality of the generated topology fi les is usually far from desirable.

There are two broad categories for the force fi elds in lipid modeling: the atomistic approach and the coarse-grained (CG) approach. The CG force fi elds, as used in the lung surfactant study in the previous section, such as the famous MARTINI model [17,27], are known for their speed and larger system sizes. Atomistic force fi elds, on the other hand, are often able to provide quantitative predictions that can be veri fi ed by experiments, and are versatile. The atomistic force fi elds can be classi fi ed into two fl avors: the all-atom ones and the united-atom ones. In an all-atom force fi eld, such as OPLS [28,29], AMBER [30–33], and CHARMM [34–36], all atoms are explicitly present in the simulation. In a united-atom force fi eld, such as the GROMOS force fi eld [37–39], the nonpolar hydrogens bonded to the carbons in an acyl chain are absorbed into the carbons to

which they are bonded, to form a *united atom* to reduce the number of interacting sites. Here, we focus on some practical issues and skills useful in obtaining good quality parametrization for lipid molecules by using one of the most widely used atomistic force fields for lipid simulations, the GROMOS force field and its derivative, the Berger lipid model [40]. It is also worth noting that the OPLS force field has also found many applications in lipid simulations (yet work remains to be done for OPLS peptide parameterization [41]). In addition, there is currently a very interesting open collaboration platform called *Matching lipid force fields with NMR data* (available at http://nmrlipids.blogspot.ca). This approach is pioneered by Markus Miettinen and Samuli Ollila that is groundbreaking and may lead to completely new developments and integration of experimental and computational lipid data.

From the practical point of view, a good way to obtain a quality parametrization for a lipid molecule is by studying and reusing mature, well-tested parametrization for other lipid molecules, which share notable amounts of parts as the lipid to be parametrized. It may, of course, be the case that no such parametrization exists. This shortcut approach has been applied to many lipid molecules with success. One of the most famous *baseline* lipid parametrizations from which many other parametrizations were derived is the DPPC parametrization [42] based on the GROMOS force field and the Berger lipid model. Many other saturated dichained lipids, including DMPC [43] and DLPC, can be easily parametrized by adding or removing repeating hydrocarbons. Borrowing the parametrization for the double-bonded hydrocarbons, this DPPC parametrization can be adapted to construct parametrization for unsaturated dichained lipids, such as DOPC, POPC, and SOPC in principle. A word of warning should be given, however: Double bonds can be tricky to parametrize and it has been shown that old parametrizations are wrong and can influence the observed physical properties of lipids and their interactions with others [44,45]. Similarly, the PC headgroup can also be substituted by other parametrized headgroups, such as the PG headgroup, to obtain parametrizations for the corresponding PG lipids [46].

If the headgroup of the lipid of interest has not been parametrized, one can use the parameter set of a force field to parametrize it. The parameter set includes equilibrium position and force constant for bonded interactions such as bond stretching, bond angle bending, proper and improper dihedral interactions, and van der Waals, radii and constants. What is usually missing in a force field for a specific headgroup is the partial charges. Quantum chemistry calculations are needed to obtain the partial charges to parametrize a headgroup. Ideally, one should apply quantum chemistry approaches to calculate the partial charges for the entire lipid. However, as the computational cost of a quantum chemistry calculation scales as the third order or even more of the number of electrons in the system, it becomes quickly intractable as the size of the lipid increases. Fortunately, the *locality* of partial charges and the *insulating* property of hydrocarbons can be employed to reduce the computational cost. The *locality* of partial charges means the partial charge of a specific site (an atom or a united atom) is only influenced heavily by its first and second bonded neighbors. One important exception is aromatic rings. In any case, an aromatic ring must be treated as a whole. The *insulating* property of hydrocarbons means one hydrocarbon can be essentially regarded as a neutrally charged dividing point to separate two independent partial charge regions. Therefore, one can perform quantum chemistry calculations for a pseudomolecule composed of a headgroup and a methyl or ethyl group. If the headgroup contains one or more hydrocarbons, one can divide the headgroup again into smaller parts and cap them with methyl or ethyl groups to form pseudomolecules. Usually the accuracy of partial charges obtained from such a pseudomolecule is within the tolerance of an MD simulation for lipids.

Quantum chemistry calculations for partial charges can be performed by using the well-known Gaussian package [47] and some open source packages such as the GAMESS family, which includes GAMESS-US [48,49] and Firefly [48,50] as its two major variants. One of the most popular basis set, for example, 6-31G* and 6-31G(d,p) [51–53], which offer both decent accuracy and acceptable computational cost, is often used for calculating the partial charges for a lipid. 6-31G* has also been employed to obtain the partial charges in the AMBER force field [54]. These basis sets usually work

well for neutral and cationic lipids. But for anionic lipids, 6-31+G* or 6-31+G(d,p) [55,56], which include diffuse functions to account for the presence of signi cant charge density that are distant from the atomic nuclei, are needed to get accurate results at the cost of slower or even dif cult convergence. To take the effect of electron correlation on partial charges into account, post-Hartree–Fock (HF) methods or density functional theory (DFT) methods are usually employed as they are generally superior to the plain HF level calculation in which electron correlation is totally neglected. The Moeller–Plesset level 2 (MP2) method, which is a post-HF method, is usually preferable as it can take most of electron correlation into account at affordable computational cost. DFT methods can also work well, provided one chooses an appropriate exchange-correlation functional (E_{xc}). The quantum chemistry packages mentioned earlier can offer four sets of partial charges, that is, those by Mulliken population analysis [57,58], Löwdin population analysis [59,60], electrostatic potential analysis (ESP) [61,62], and natural population analysis (NPA) [63–65]. NPA can only be done by the natural bond orbital (NBO) module [65], which exists as a plug-in for all the major quantum chemistry packages. Once one obtains the four sets of partial charges, one should rst use one's chemical instinct to judge which set is most reasonable. Our experience shows that usually, the NPA scheme is the choice as it is not sensitive to the choice of basis set, theory level, or initial structure of the molecule being investigated. But the choice of partial charge scheme could differ from case to case. In principle, one should also employ polarized continuum model (PCM) [66–69] to re ect the in uence of the aqueous environment on partial charges. However, our experience shows the use of PCM makes negligible difference for partial charges of the molecules for biological or physiological simulations.

Quantum chemistry calculations for partial charges usually take two steps. First, one uses the plain HF level calculation to perform geometry optimization for the molecule being investigated and obtain the *equilibrium* structure. We put a double quote to encompass the word equilibrium, because the geometry optimization usually ends up in a local minimum or even a saddle point on the potential energy surface as the global minimum is extremely dif cult to reach if possible at all. This is caused by the high dimensional and very complex potential energy surface landscape of any molecule of decent size. The point of performing this step is getting a structure reasonably close to the real equilibrium structure for the second quantum chemistry calculation step, and in real MD trajectories, molecules are always close to their equilibrium structures but seldom sit there. The second step involves using the optimized structure obtained in the rst step to perform single point calculation at either MP2 level or with a DFT method to account for electron correlation. Our experience shows the partial charges obtained by using a MP2 level or DFT calculation are distinguishable from those from the plain HF level calculation, but reasonably close.

One may encounter the dif cult situation in which one bonded interaction in the molecule being parametrized has not been parametrized in a speci c force eld. One obvious approach is to look for experimental results to nd the equilibrium position and force constant for it. One can also resort to quantum chemistry calculations to perform a scan of the potential energy surface on the dimension of interest. In the following example (Figure 11.4), the angle bending interaction between CH_2–(C═O)–C(benzene) is not parametrized in the GROMOS force eld [39]. The rst step to parametrize it using

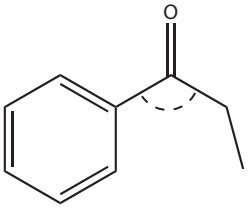

FIGURE 11.4 Diagram for a pseudomolecule for parametrizing the angle bending interaction between CH_2–(C═O)–C(benzene).

the harmonic oscillator approximation is capping CH_2 with CH_3 (methyl group) to form a pseudomolecule. To facilitate the parametrization, one would better convert the structure representation of this pseudomolecule from Cartesian to internal coordinates (Z-matrix representation), which can be accomplished by using chemical visualization programs such as MacMolPlt [70]. Then one can generate a set of input files for quantum chemistry calculations with single point structures represented by Z-matrix and with varying CH_2–(C═O)–C angles, which should cover the guessed equilibrium angle. This set of quantum chemistry calculations usually can give a set of system energies, which can be almost perfectly fitted to a parabola against the varying CH_2–(C═O)–C angles. From the fitting, one can retrieve the equilibrium angle and force constant for this angle bending interaction.

11.4 SIMULATION BOX SETUP

Once parametrization for all molecules has been obtained; the next step for the simulation is to construct a simulation box, which consists of all the components needed and has the appropriate geometric configuration. In theory, any box type that can fill up the entire space with periodic boundary condition can be used for monolayer simulations, including some perhaps bizarre sounding box types like rhombic dodecahedron or truncated octahedron. For the easy of analysis and practical reasons, the simplest rectangular box type is almost always used unless there are some special requirements.

For monolayer at air/water interface simulations, there are two popular geometrical configuration setups (see Figure 11.5). In Figure 11.5a, the simulated monolayer is placed at the interface between the water and air phases, and a wall potential is applied to the bottom of the water phase to prevent molecules from escaping. The water slab should be thick enough to allow recovery of bulk water property for the region that has a direct effect on the monolayer [71]. Another very popular configuration is displayed in Figure 11.5b where two symmetrical monolayers are separated by a water slab thick enough to restore bulk water property in the middle and hence prevent interactions between these two monolayers [72]. Caution should be taken when one uses the setup in Figure 11.5a with the constant particle number, pressure and temperature (NPT) ensemble, or in a situation in which severe buckling may develop, as the varying box size or monolayer geometry may interfere with the wall potential and cause artifacts.

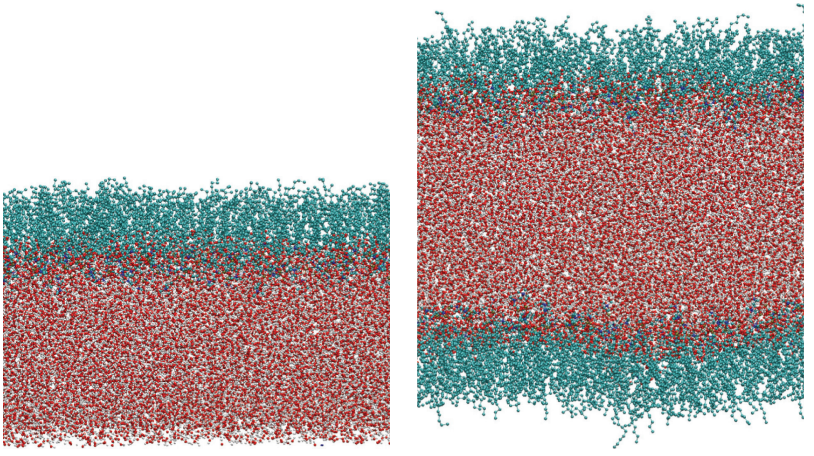

FIGURE 11.5 Two types of simulation box setup for monolayers at the air/water interface. (a) A wall potential is applied to prevent water from escaping. (b) Symmetrical monolayers separated by a thick water slab. Monolayers displayed here consist of DPPC lipids modeled by the GROMOS force field and the Berger lipid model.

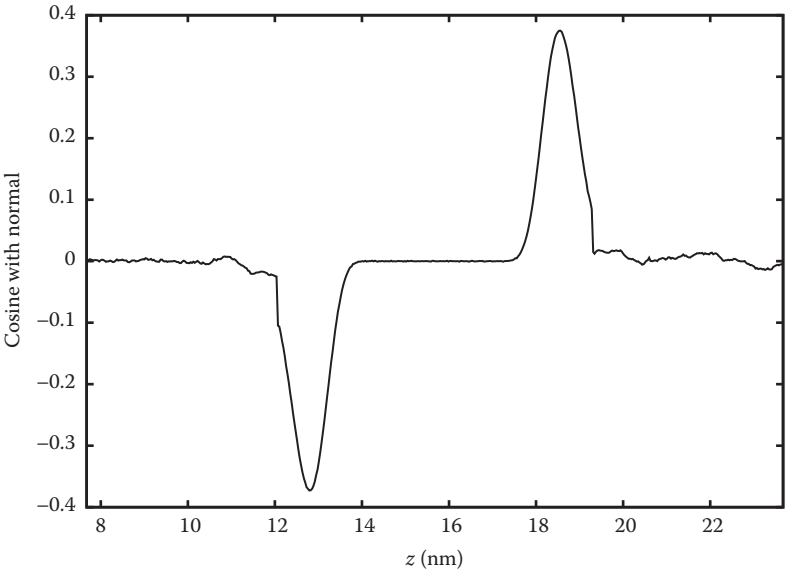

FIGURE 11.6 Water dipole orientation for the symmetrical con guration in Figure 11.5b. The two symmetrical peaks correspond to the phosphate region in the DPPC headgroup, which signi cantly reorients water dipole. Bulk water property rapidly resumes away from the headgroup region. The ripples in the lipid chain region and in the air phase are caused by small number of water molecules that have escaped from the water slab.

One way to check if the water slab in Figure 11.5b is thick enough is to calculate water dipole orientation along the z-axis and calculate the Debye screening length. In the vicinity of the polar headgroups of the monolayers, water dipole orientation is distinctively different from that in bulk water region, which should be isotropic. With either con guration, the air phase (essentially vacuum in most simulations) needs to be thick enough to prevent the interactions between the simulated system and its periodic images in z-direction (Figure 11.6).

11.5 RUNNING MONOLAYER SIMULATIONS

Once the simulation box has been constructed, the production simulations are usually the least complicated step compared to parametrization or analysis (which will be discussed in detail in the following later). Modern MD packages, such as GROMACS [73], NAMD [74], and AMBER [75], usually provide reliable default parameter settings and excellent documentation. One must, however, always pay attention to the particular demands of the system and verify that the behavior is physically correct [76]. Typically, one needs to conduct trial simulations to verify the choice of parameters against existing experiments or other simulation results.

Usually monolayer simulations start with the energy minimization step. Steep descent and conjugate gradient (CG) methods are the most popular choices. This step relaxes the energy introduced by the arti cial system setup, which could otherwise make the following dynamic simulation steps unstable. Failing to complete the minimization step usually indicates serious issues in either parametrization or simulation box setup or both.

Depending on the goals one wants to achieve with a monolayer simulation, the next step could be either a constant temperature (*NVT*) simulation that comprises of both the equilibration stage and the production stage, or a series of *NVT* simulations or constant temperature constant pressure (*NPT*) simulations for equilibration followed by a production of *NPT* simulation. The choice of thermostat and/or barostat determines the quality of *NVT* or *NPT* simulations to a large extent.

Popular thermostats include Nosé-Hoover [77,78] or Nosé-Hoover chains [79], Berendsen thermostat or its variants [80], Andersen thermostat [81], and the increasingly popular V-Rescale thermostat [82], which has proven to be suitable for both equilibration and production simulations [83]. Popular barostats include Berendsen coupling [80], which is very useful for situations where the system is far from equilibration as it provides rst-order decaying toward equilibrium, and the Parrinello–Rahman coupling [84] that serves the production stage very well and is generally the recommended method.

In the past, treating long-ranged Coulombic interactions were computationally intensive and tricky to handle. The particle mesh Ewald (PME) algorithm [85] is becoming the *de facto* standard treatment for Coulombic interactions as it offers both satisfactory accuracy and very decent ef - ciency [86–90], provided one chooses appropriate cutoff ranges. The choice of real-space range is usually less important when PME is used than with other algorithms that treat Coulombic interactions such as reaction eld [91], since in PME, the real-space cutoff is no more than a division of computational burden into a real-space part and a reciprocal space part. The lower sensitivity to the choice of cutoff range in PME is another advantage. Recent reviews are provided in Refs. [89,90]. Our other contribution in this book also contains a detailed discussion of electrostatic interactions when interfaces are present (see Chapter 6).

11.6 ANALYSIS AND A CASE STUDY FOR DPPC/CTAB MONOLAYERS

In this section, we discuss both the conventional analysis that can be relatively easily done and some advanced analysis techniques, which have been recently developed in the context of monolayer simulations. As shown in Figures 11.5b and 11.7, both pure DPPC monolayers and DPPC/CTAB mixtures were simulated by employing the symmetrical con guration setup [72]. Each monolayer in the simulation box consists of 128 lipids. Cetyltrimethylammonium bromide (CTAB) is a cationic surfactant [92]. It has a trimethyl ammonium headgroup and a lipid chain of 16 hydrocarbons. A series of *NVT* simulations with various simulation box sizes at various CTAB molar fractions were conducted.

Snapshots along the trajectory are often an intuitive and important way to gauge how the simulation evolves in time. Figure 11.7 displays snapshots at the end of 1 μs trajectories for three monolayers with various CTAB molar fractions. The visualizations were obtained by using the VMD [93,94] software, possibly the most popular MD visualization tool. Severe buckling occurs in the

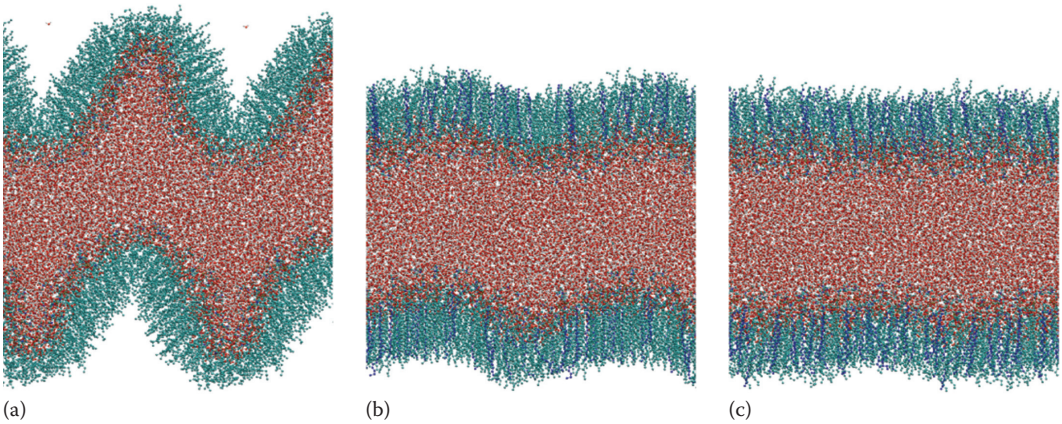

FIGURE 11.7 Pure DPPC monolayer and DPPC/CTAB mixtures at area per lipid 0.4 nm^2. (a) High surface pressure at very low area per lipid induces buckling in pure DPPC monolayer. (b) 20% cationic CTAB (deep blue) with 80% DPPC mixture has only very wild surface undulation. (c) 30% Cationic CTAB (deep blue) with 70% DPPC mixture resumes at geometry even at very low area per lipid.

pure DPPC monolayer (Figure 11.7a) at a low area per lipid 0.4 nm^2, which indicates high surface pressure. The monolayer with 20% CTAB displays much milder buckling and with 30% CTAB, buckling almost disappears. This indicates CTAB stabilizes the at geometry of DPPC monolayers, especially with high surface pressure.

The goals of conducting an MD simulation can be categorized into studying statistical properties and investigating dynamical processes. Before taking statistics, one must ensure equilibrium has been reached and that the trajectories from the equilibration have been discarded from the analysis. The most common approach to judge if the system has entered equilibrium is to investigate the trend of various energies, including total, kinetic, potential, and other energies belonging to various degrees of freedom. If at least one of them is still displaying a systematic increase or decrease, the system is still not in equilibrium. This is, however, not a suf cient criterion and other quantities, for example, the number of hydrogen bonds, must be monitored. In addition, analysis of uctuations is often a useful way to analyze equilibrium. Analysis of lateral diffusion of lipids (effective mixing) is another important quantity. The lateral diffusion coef cient can be evaluated by

$$D_\alpha = \lim_{t\to\infty} \frac{1}{4t}\langle r^2(t)\rangle = \lim_{t\to\infty} \frac{1}{4tN_\alpha} \sum_{i=1}^{N_\alpha} \langle r_i^2(t)\rangle, \tag{11.1}$$

where

the subscript α denotes a speci c type of lipid. In this case study, it is either DPPC or CTAB.
$\langle r_i^2(t)\rangle$ is the average squared lateral displacement of the ith lipid belonging to type α at time t
N_α is the total number of lipids of type α in the system

The motion of the center of mass of the corresponding lea et needs to be removed from $r_i^2(t)$.

One of the most important characterizations for the behavior of monolayers is the surface tension/pressure to area per lipid isotherms. From the pressure tensor in the simulation box, the surface tension of a monolayer can be evaluated [95] as

$$\gamma = \langle (P_N - P_L)\cdot L_z\rangle/2 = \langle (P_N - P_L)\rangle \cdot L_z/2, \tag{11.2}$$

where

L_z is the box size in z-direction
$P_N = P_{zz}$ is the normal pressure and the third diagonal component of the pressure tensor
$P_L = (P_{xx} + P_{yy})/2$ is the lateral pressure
P_{xx} and P_{yy} are the rst and second components of the pressure tensor

The brackets denote averaging over time. The second equality applies only to *NVT* simulations where the box size in z-direction is a constant, which applies to the case study here.

To get a more direct comparison between simulations and experimental data, the surface pressure of a monolayer can be evaluated, which can be accomplished by deducting the surface tension of the monolayer from the bare air/water surface tension under the same condition:

$$\Pi(A_L, T) = \gamma_0(T) - \gamma(A_L, T), \tag{11.3}$$

where $\gamma_0 \equiv \gamma_0(T)$ is the bare water/air surface tension, which is a function of temperature, and both Π and γ are functions of the area per lipid A_L and temperature.

However, no water model can reproduce the real bare air/water surface tension for a broad range of temperature, which might be used in biological or physiological simulations.

Therefore, instead of using experimental data for bare air/water surface tension, the simulated values by the speci c water model used in a simulation should be employed to ensure consistency. In addition, density pro ling is a valuable tool to investigate the relative positioning of all relevant components in the simulation box and the change of it caused by other factors (Figures 11.8 through 11.10).

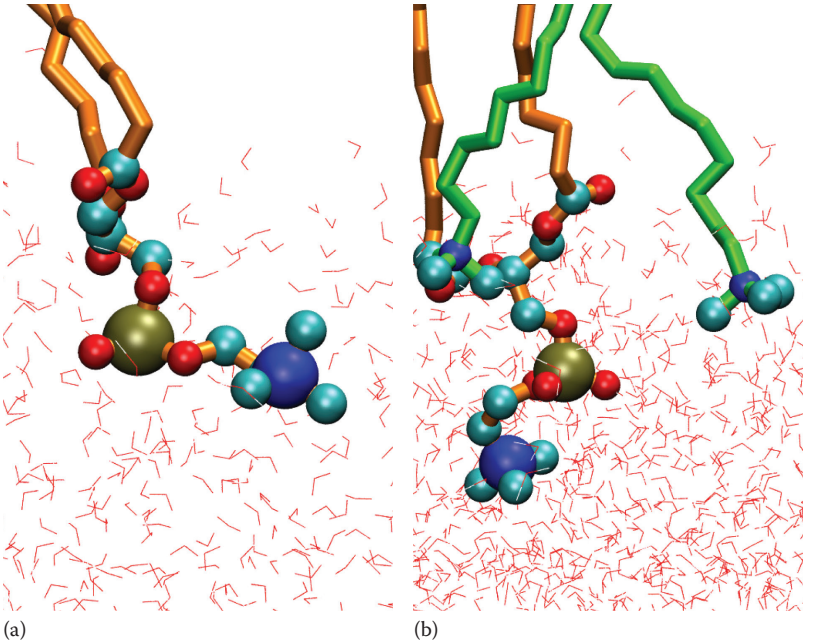

FIGURE 11.8 Phosphorus (the large tan atom)–nitrogen (the large blue atom) vector in PC headgroups reoriented by neighboring cationic CTAB. (a) The P-N vector of DPPC is oriented almost parallel to the monolayer plane. (b) The cationic CTAB (green lipid tail) essentially reorients the P-N vector of DPPC.

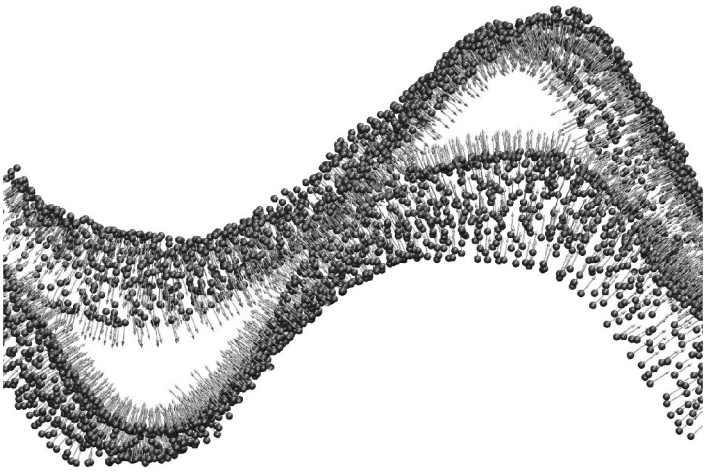

FIGURE 11.9 The normal vectors (arrows) for highly buckled DPPC monolayers separated by a water slab. Each monolayer has 2048 DPPCs. Water is disabled in visualization for clarity. Phosphates were chosen to approximate the interface between water and DPPC monolayers. The normal vectors always point toward water.

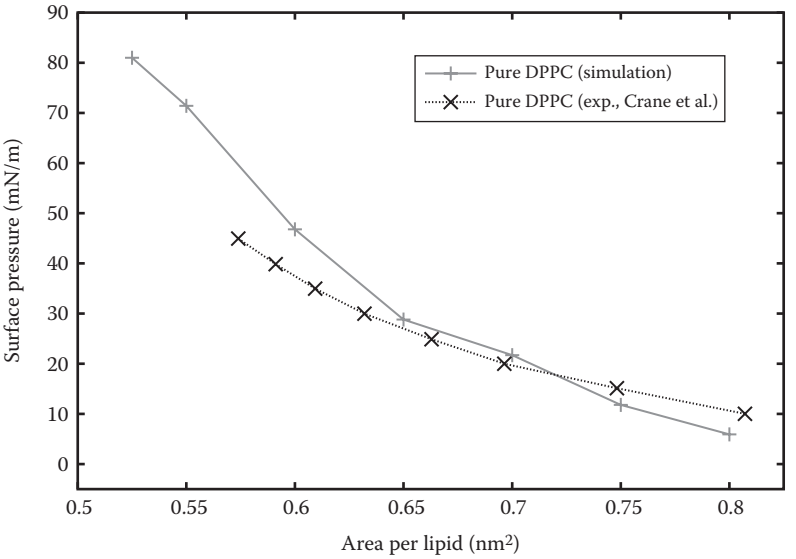

FIGURE 11.10 Surface pressure-area per lipid isotherms for pure DPPC monolayers simulated at 323 K. (The experimental data were obtained by Crane, J.M. et al., *Biophys. J.*, 77, 3134, 1999.)

11.7 DISCUSSION AND CONCLUSIONS

In this chapter, we have provided a detailed discussion of how to set up monolayer simulations, the caveats and various technical details as well as software commonly used for such simulations. Our aim was not to provide a comprehensive review of the vast literature on the topic but rather to provide a fairly hands-on approach to help the interested readers to set up, run, and analyze their own simulations.

ACKNOWLEDGMENTS

We thank Dr. Toby Zeng for fruitful discussion on quantum chemistry calculations and Prof. Pierre-Nicolas Roy for providing some of the computational resources. Computational resources were provided by SharcNet (https://www.sharcnet.ca/), the WestGrid HPC Consortium, the SciNet Consortium, and Compute Canada. Financial support was provided by the Waterloo Institute for Nanotechnology Nanofellowship program (BL), the University of Waterloo (MK), the Ontario Government (BL), and Natural Sciences and Engineering Research Council of Canada (NSERC; MK).

REFERENCES

1. D. B. Kittelson. Engines and nanoparticles: A review. *J Aerosol Sci*, 29:575–588, 1998.
2. Z. D. Ristovski, L. Morawska, N. D. Bo nger, and J. Hitchins. Submicrometer and supermicrometer particulate emission from spark ignition vehicles. *Environ Sci Technol*, 32:3845–3852, 1998.
3. M. M. Maricq, D. H. Podsiadlik, and R. E. Chase. Examination of the size-resolved and transient nature of motor vehicle particle emissions. *Environ Sci Technol*, 33:1618–1626, 1999.
4. L. Morawska, N. D. Bo nger, L. Kocis, and A. Nwankwoala. Submicrometer and supermicremeter particles from diesel vehicle emissions. *Environ Sci Technol*, 32:2033–2042, 1998.
5. C. Buzea, I. I. Pacheco, and K. Robbie. Nanomaterials and nanoparticles: Sources and toxicity. *Biointerphases*, 2:Mr17–Mr71, 2007.
6. G. Oberdorster, E. Oberdorster, and J. Oberdorster. Nanotoxicology: An emerging discipline evolving from studies of ultra ne particles. *Environ Health Perspect*, 113:823–839, 2005.

7. G. Oberdorster, Z. Sharp, V. Atudorei, A. Elder, R. Gelein, W. Kreyling, and C. Cox. Translocation of inhaled ultra ne particles to the brain. *Inhal Toxicol*, 16:437–445, 2004.
8. C. W. Lam, J. T. James, R. McCluskey, S. Arepalli, and R. L. Hunter. A review of carbon nanotube toxicity and assessment of potential occupational and environmental health risks. *Crit Rev Toxicol*, 36:189–217, 2006.
9. A. Seaton, W. MacNee, K. Donaldson, and D. Godden. Particulate air pollution and acute health effects. *Lancet*, 345:176–8, 1995.
10. G. Oberdorster, J. Ferin, and B. E. Lehnert. Correlation between particle size, in vivo particle persistence, and lung injury. *Environ Health Perspect*, 102(Suppl. 5):173–179, 1994.
11. D.F. Merlo, S. Garattini, U. Gelatti, C. Simonati, L. Covolo, M. Ceppi, and F. Donato. A mortality cohort study among workers in a graphite electrode production plant in Italy. *Occup Environ Med*, 61:e9, 2004.
12. C.G. Uragoda. A cohort study of graphite workers in Sri Lanka. *Occup Med (Lond)*, 47:269–272, 1997.
13. A. Huczko, H. Lange, E. Calko, H. Grubek-Jaworska, and P. Droszcz. Physiological testing of carbon nanotubes: Are they asbestos-like? *Fullerene Sci Technol*, 9:251–254, 2001.
14. Z. Wang and S. Yang. Effects of fullerenes on phospholipid membranes: A langmuir monolayer study. *Chemphyschem*, 10:2284–2289, 2009.
15. C. C. Chiu, W. Shinoda, R. H. DeVane, and S. O. Nielsen. Effects of spherical fullerene nanoparticles on a dipalmitoyl phosphatidylcholine lipid monolayer: A coarse grain molecular dynamics approach. *Soft Matter*, 8:9610–9616, 2012.
16. J. Goerke. Pulmonary surfactant: Functions and molecular composition. *Biochim Biophys Acta*, 1408:79–89, 1998.
17. S. J. Marrink, A. H. de Vries, and A. E. Mark. Coarse grained model for semiquantitative lipid simulations. *J Phys Chem B*, 108(2):750–760, January 2004.
18. N. Nisoh, M. Karttunen, L. Monticelli, and J. Wong-Ekkabut. Lipid monolayer disruption caused by aggregated carbon nanoparticles. *Rsc Adv*, 5:11676–11685, 2015.
19. S. Baoukina, L. Monticelli, S. J. Marrink, and D. P. Tieleman. Pressure-area isotherm of a lipid monolayer from molecular dynamics simulations. *Langmuir*, 23:12617–12623, 2007.
20. J. Barnoud, L. Urbini, and L. Monticelli. C60 fullerene promotes lung monolayer collapse. *J R Soc Interface*, 12:20140931, 2015.
21. J. Wong-Ekkabut, S. Baoukina, W. Triampo, I. M. Tang, D. P. Tieleman, and L. Monticelli. Computer simulation study of fullerene translocation through lipid membranes. *Nat Nanotechnol*, 3:363–368, 2008.
22. F. R. Poulain and J. A. Clements. Pulmonary surfactant therapy. *West J Med*, 162:43–50, 1995.
23. J. A. Clements. Pulmonary edema and permeability of alveolar membranes. *Arch Environ Health*, 2:280–283, 1961.
24. J. A. Clements. Surface phenomena in relation to pulmonary function. *Physiologist*, 5:11–28, 1962.
25. B. Robertson and H. L. Halliday. Principles of surfactant replacement. *Biochim Biophys Acta*, 1408:346–361, 1998.
26. A. W. Schüttelkopf and D. M. F. van Aalten. PRODRG: A tool for high-throughput crystallography of protein-ligand complexes. *Acta Crystallogr D Biol Crystallogr*, 60(Pt 8):1355–1363, August 2004.
27. S. J. Marrink and D. Peter Tieleman. Perspective on the martini model. *Chem Soc Rev*, 42:6801, 2013.
28. W. L. Jorgensen, D. S. Maxwell, and J. Tirado-Rives. Development and testing of the OPLS all-atom force eld on conformational energetics and properties of organic liquids. *J Am Chem Soc*, 118(45):11225–11236, January 1996.
29. G. A. Kaminski, R. A. Friesner, J. Tirado-Rives, and W. L. Jorgensen. Evaluation and reparametrization of the OPLS-AA force eld for proteins via comparison with accurate quantum chemical calculations on peptides †. *J Phys Chem B*, 105(28):6474–6487, July 2001.
30. W. D. Cornell, P. Cieplak, C. I. Bayly, I. R. Gould, K. M. Merz, D. M. Ferguson, D. C. Spellmeyer, T. Fox, J. W. Caldwell, and P. A. Kollman. A second generation force eld for the simulation of proteins, nucleic acids, and organic molecules. *J Am Chem Soc*, 117(19):5179–5197, May 1995.
31. J. Wang, P. Cieplak, and P. A. Kollman. How well does a restrained electrostatic potential (RESP) model perform in calculating conformational energies of organic and biological molecules? *J Comput Chem*, 21(12):1049–1074, September 2000.
32. E. J. Sorin and V. S. Pande. Exploring the helix-coil transition via all-atom equilibrium ensemble simulations. *Biophys J*, 88(4):2472–2493, April 2005.
33. Y. Duan, C. Wu, S. Chowdhury, M. C. Lee, G. Xiong, W. Zhang, R. Yang et al. A point-charge force eld for molecular mechanics simulations of proteins based on condensed-phase quantum mechanical calculations. *J Comput Chem*, 24(16):1999–2012, December 2003.

34. E. Neria, S. Fischer, and M. Karplus. Simulation of activation free energies in molecular systems. *J Chem Phys*, 105(5):1902, 1996.
35. A. D. MacKerell, D. Bashford, M. Bellott, R. L. Dunbrack, J. D. Evanseck, M. J. Field, S. Fischer et al. All-atom empirical potential for molecular modeling and dynamics studies of proteins. *J Phys Chem B*, 102(18):3586–3616, April 1998.
36. A. D. Mackerell, M. Feig, and C. L. Brooks. Extending the treatment of backbone energetics in protein force elds: Limitations of gas-phase quantum mechanics in reproducing protein conformational distributions in molecular dynamics simulations. *J Comput Chem*, 25(11):1400–1415, August 2004.
37. W. R. P. Scott, P. H. Hünenberger, I. G. Tironi, A. E. Mark, S. R. Billeter, J. Fennen, A. E. Torda, T. Huber, P. Krüger, and W. F. van Gunsteren. The GROMOS biomolecular simulation program package. *J Phys Chem A*, 103(19):3596–3607, May 1999.
38. X. Daura, A. E. Mark, and W. F. van Gunsteren. Parametrization of aliphatic CHn united atoms of GROMOS96 force eld. *J Comput Chem*, 19(5):535–547, 1998.
39. C. Oostenbrink, A. Villa, A. E. Mark, and W. F. van Gunsteren. A biomolecular force eld based on the free enthalpy of hydration and solvation: The GROMOS force- eld parameter sets 53A5 and 53A6. *J Comput Chem*, 25:1656–1676, 2004.
40. O. Berger, O. Edholm, and F. Jahnig. Molecular dynamics simulations of a uid bilayer of dipalmitoylphosphatidylcholine at full hydration, constant pressure, and constant temperature. *Biophys J*, 72:2002–2013, 1997.
41. E. A. Cino, W.-Y. Choy, and M. Karttunen. Comparison of secondary structure formation using 10 different force elds in microsecond molecular dynamics simulations. *J Chem Theory Comput*, 8:2725–2740, 2012.
42. P. Tieleman, Biocomputing Group, University of Calgary, http://wcm.ucalgary.ca/tieleman/downloads. Accessed on February 22, 2015.
43. A. A. Gurtovenko, M. Patra, M. Karttunen, and I. Vattulainen. Cationic DMPC/DMTAP lipid bilayers: Molecular dynamics study. *Biophys J*, 86(6):3461–3472, June 2004.
44. M. Bachar, P. Brunelle, D. Peter Tieleman, and A. Rauk. Molecular dynamics simulation of a polyunsaturated lipid bilayer susceptible to lipid peroxidation. *J Phys Chem B*, 108:7170–7179, 2004.
45. H. Martinez-Seara, T. Rog, M. Karttunen, R. Reigada, and I. Vattulainen. In uence of cis double-bond parametrization on lipid membrane properties: How seemingly insigni cant details in force- eld change even qualitative trends. *J. Chem. Phys.*, 129:105103, 2008.
46. W. Zhao, T. Róg, A. A. Gurtovenko, I. Vattulainen, and M. Karttunen. Atomic-scale structure and electrostatics of anionic palmitoyloleoylphosphatidylglycerol lipid bilayers with Na+ counterions. *Biophys J*, 92(4):1114–1124, February 2007.
47. M. J. Frisch, G. W. Trucks, H. B. Schlegel, G. E. Scuseria, M. A. Robb, J. R. Cheeseman, J. A. Montgomery, Jr. et al. Gaussian 03, Revision C.02. Gaussian, Inc., Wallingford, CT, 2004.
48. M. W. Schmidt, K. K. Baldridge, J. A. Boatz, S. T. Elbert, M. S. Gordon, J. H. Jensen, S. Koseki et al. Montgomery. General atomic and molecular electronic structure system. *J Comput Chem*, 14(11):1347–1363, November 1993.
49. M. S. Gordon and M. W. Schmidt. Advances in electronic structure theory: GAMESS a decade later. In C. E. Dykstra, G. Frenking, K. S. Kim, and G. E. Scuseria, eds., *Theory and Application of Computational Chemistry*: *The First Forty Years*, pp. 1167–1189. Elsevier, Amsterdam, the Netherlands, 2005.
50. A. A. Granovsky. Fire y quantum chemistry package version 8. http://classic.chem.msu.su/gran/ re y/index.html. Accessed on November 10, 2014.
51. R. Ditch eld, W. J. Hehre, and J. A. Pople. Self-consistent molecular-orbital methods. IX. An extended gaussian-type basis for molecular-orbital studies of organic molecules. *J. Chem. Phys.*, 54(2):724, 1971.
52. W. J. Hehre, R. Ditch eld, and J. A. Pople. Self-consistent molecular orbital methods. XII. Further extensions of gaussian-type basis sets for use in molecular orbital studies of organic molecules. *J. Chem. Phys.*, 56(5):2257, 1972.
53. P. C. Hariharan and J. A. Pople. The in uence of polarization functions on molecular orbital hydrogenation energies. *Theor. Chem. Acc.*, 28:213–222, 1973.
54. V. Hornak, R. Abel, A. Okur, B. Strockbine, A. Roitberg, and C. Simmerling. Comparison of multiple Amber force elds and development of improved protein backbone parameters. *Proteins*, 65(3):712–725, November 2006.
55. G. A. Petersson, A. Bennett, T. G. Tensfeldt, M. A. Al-Laham, W. A. Shirley, and J. Mantzaris. A complete basis set model chemistry. I. The total energies of closed-shell atoms and hydrides of the rst-row elements. *J. Chem. Phys.*, 89(4):2193, 1988.

56. G. A. Petersson and M. A. Al-Laham. A complete basis set model chemistry. II. Open-shell systems and the total energies of the first-row atoms. *J. Chem. Phys.*, 94(9):6081, 1991.
57. R. S. Mulliken. Electronic population analysis on LCAO [Single Bond] MO molecular wave functions. I. *J. Chem. Phys.*, 23(10):1833, 1955.
58. R. S. Mulliken. Criteria for the construction of good self-consistent- field molecular orbital wave functions, and the significance of LCAO-MO population analysis. *J. Chem. Phys.*, 36(12):3428, 1962.
59. P.-O. Löwdin. On the non-orthogonality problem. *Adv. Quantum Chem.*, 5:185–199, 1970.
60. L.C. Cusachs and P. Politzer. On the problem of defining the charge on an atom in a molecule. *Chem. Phys. Lett.*, 1(11):529–531, January 1968.
61. D. E. Williams. *Net Atomic Charge and Multipole Models for the Ab Initio Molecular Electric Potential*, pp. 219–271. John Wiley Sons, Inc., Weinheim, Germany, 2007.
62. B. Wang and G. P. Ford. Atomic charges derived from a fast and accurate method for electrostatic potentials based on modified AM1 calculations. *J. Comput. Chem.*, 15(2):200–207, February 1994.
63. K. C. Gross, P. G. Seybold, and C. M. Hadad. Comparison of different atomic charge schemes for predicting pKa variations in substituted anilines and phenols. *Int. J. Quantum Chem.*, 90(1):445–458, August 2002.
64. R. S. Vareková, S. Geidl, C.-M. Ionescu, O. Skrehota, M. Kudera, D. Sehnal, T. Bouchal, R. Abagyan, H. J. Huber, and J. Koca. Predicting pK(a) values of substituted phenols from atomic charges: Comparison of different quantum mechanical methods and charge distribution schemes. *J. Chem. Inf. Model.*, 51(8):1795–1806, August 2011.
65. E. D. Glendening, J. K. Badenhoop, A. E. Reed, J. E. Carpenter, J. A. Bohmann, C. M. Morales, and F. Weinhold. Nbo 5.9. Theoretical Chemistry Institute, University of Wisconsin, Madison, WI, 2012. http://www.chem.wisc.edu/~nbo5, 2012.
66. S. Miertuš, E. Scrocco, and J. Tomasi. Electrostatic interaction of a solute with a continuum. A direct utilizaion of ab initio molecular potentials for the prevision of solvent effects. *Chem. Phys.*, 55(1):117–129, February 1981.
67. J. Tomasi and M. Persico. Molecular interactions in solution: An overview of methods based on continuous distributions of the solvent. *Chem. Rev.*, 94(7):2027–2094, November 1994.
68. R. Cammi and J. Tomasi. Remarks on the use of the apparent surface charges (ASC) methods in solvation problems: Iterative versus matrix-inversion procedures and the renormalization of the apparent charges. *J. Comput. Chem.*, 16(12):1449–1458, 1995.
69. J. Tomasi, B. Mennucci, and R. Cammi. Quantum mechanical continuum solvation models. *Chem. Rev.*, 105(8):2999–3093, August 2005.
70. B. M. Bode and M. S. Gordon. Macmolplt: A graphical user interface for GAMESS. *J. Mol. Graph. Model.*, 16(3):133–138, June 1998.
71. Y. N. Kaznessis, S. Kim, and R. G. Larson. Simulations of zwitterionic and anionic phospholipid monolayers. *Biophys. J.*, 82(4):1731–1742, April 2002.
72. B. Liu, M. I. Hoopes, and M. Karttunen. Molecular dynamics simulations of DPPC/CTAB monolayers at the air/water interface. *J. Phys. Chem. B*, 118(40):11723–11737, October 2014.
73. B. Hess, C. Kutzner, D. van der Spoel, and E. Lindahl. GROMACS 4: Algorithms for highly efficient, load-balanced, and scalable molecular simulation. *J. Chem. Theory Comput.*, 4:435–447, 2008.
74. J. C. Phillips, R. Braun, W. Wang, J. Gumbart, E. Tajkhorshid, E. Villa, C. Chipot, R. D. Skeel, L. Kalé, and K. Schulten. Scalable molecular dynamics with NAMD. *J. Comput. Chem.*, 26(16):1781–1802, December 2005.
75. D. A. Case, T. E. Cheatham, T. Darden, H. Gohlke, R. Luo, K. M. Merz, A. Onufriev, C. Simmerling, B. Wang, and R. J. Woods. The Amber biomolecular simulation programs. *J. Comput. Chem.*, 26(16):1668–1688, December 2005.
76. J. Wong-Ekkabut, M. S. Miettinen, C. Dias, and M. Karttunen. Static charges cannot drive a continuous flow of water molecules through a carbon nanotube. *Nat. Nanotechnol.*, 5:555–557, 2010.
77. S. Nose. A unified formulation of the constant temperature molecular dynamics methods. *J. Chem. Phys.*, 81(1):511, 1984.
78. W. G. Hoover. Canonical dynamics: Equilibrium phase-space distributions. *Phys. Rev. A*, 31:1695–1697, March 1985.
79. G. J. Martyna, M. L. Klein, and M. Tuckerman. Nose–Hoover chains: The canonical ensemble via continuous dynamics. *J. Chem. Phys.*, 97(4):2635, 1992.
80. H. J. C. Berendsen, J. P. M. Postma, W. F. van Gunsteren, A. DiNola, and J. R. Haak. Molecular dynamics with coupling to an external bath. *J. Chem. Phys.*, 81(8):3684, 1984.
81. H. C. Andersen. Molecular dynamics simulations at constant pressure and/or temperature. *J. Chem. Phys.*, 72(4):2384, 1980.

82. G. Bussi, D. Donadio, and M. Parrinello. Canonical sampling through velocity rescaling. *J. Chem. Phys.*, 126:014101, 2007.
83. J. Wong-Ekkabut and M. Karttunen. Assessment of common simulation protocols for simulations of nanopores, membrane proteins, and channels. *J. Chem. Theory Comput.*, 8(8):2905–2911, August 2012.
84. M. Parrinello. Polymorphic transitions in single crystals: A new molecular dynamics method. *J. Appl. Phys.*, 52(12):7182, 1981.
85. U. Essmann, L. Perera, M. L. Berkowitz, T. Darden, H. Lee, and L. G. Pedersen. A smooth particle mesh Ewald method. *J. Chem. Phys.*, 103(19):8577, 1995.
86. D. M. York, T. A. Darden, and L. G. Pedersen. The effect of long-range electrostatic interactions in simulations of macromolecular crystals: A comparison of the Ewald and truncated list methods. *J. Chem. Phys.*, 99(10):8345, 1993.
87. M. Patra, M. Karttunen, M. T. Hyvönen, E. Falck, P. Lindqvist, and I. Vattulainen. Molecular dynamics simulations of lipid bilayers: Major artifacts due to truncating electrostatic interactions. *Biophys. J.*, 84(6):3636–3645, June 2003.
88. M. Patra, M. T. Hyvönen, E. Falck, M. Sabouri-Ghomi, I. Vattulainen, and M. Karttunen. Long-range interactions and parallel scalability in molecular simulations. *Comput. Phys. Commun.*, 176(1):14–22, January 2007.
89. M. Karttunen, J. Rottler, I. Vattulainen, and C. Sagui. Electrostatics in Biomolecular Simulations: Where Are We Now and Where Are We Heading? *Current Topics in Membranes,* 60:49–89, 2008.
90. G. A. Cisneros, M. Karttunen, P. Ren, and C. Sagui. Classical electrostatics for biomolecular simulations. *Chem. Rev.*, 114(1):779–814, January 2014.
91. J.A. Barker and R.O. Watts. Monte Carlo studies of the dielectric properties of water-like models. *Mol. Phys.*, 26(3):789–792, August 1973.
92. Ch. J. Johnson, E. Dujardin, S. A. Davis, C. J. Murphy, and S. Mann. Growth and form of gold nanorods prepared by seed-mediated, surfactant-directed synthesis. *J. Mater. Chem.*, 12(6):1765–1770, May 2002.
93. W. Humphrey, A. Dalke, and K. Schulten. VMD: Visual molecular dynamics. *J. Mol. Graph.*, 14(1):33–38, 27–28, February 1996.
94. J. Stone. An ef cient library for parallel ray tracing and animation. Technical report, In *Intel Supercomputer Users Group Proceedings*, Sandia National Laboratory, Albequerque NM, 1995.
95. S. Baoukina, S. J. Marrink, and D. P. Tieleman. Structure and dynamics of lipid monolayers: Theory and applications. In R. Faller, T. Jue, M. L. Longo, and S. H. Risbud, eds., *Biomembrane Frontiers*: *Nanostructures, Models and the Design of Life*, pp. 75–99. Humana Press, New York, 2009.
96. J. M. Crane, G. Putz, and S. B. Hall. Persistence of phase coexistence in disaturated phosphatidylcholine monolayers at high surface pressures. *Biophys. J.*, 77(6):3134–3143, December 1999.